Journal of Agricultural Engineering
https://www.agroengineering.org/

Optimization of microclimate uniformity in a multi-layer container-type strawberry smart farm using CFD and the Taguchi method

Min Gyu Jung,[1,2*] Md. Didarul Islam,[3*] Ji Min Jeong,[1] Byeong Jun Jeon,[4] Yong Kab Lee,[5] Min-Gyu Jeon,[6] Hyoung-Ho Kim[7]

[1]Department of Mechanical Engineering,Gyeongsang National University, Jinju
[2]Department of Horticulture; Gyeongsang National University, Jinju
[3]Graduate School of Mechanical and Aerospace Engineering, Gyeongsang National University, Jinju
[4]Jeres Farm, Yesan
[5]SIMEX Corporation, Seoul
[6]Department of Mechanical System Engineering, Republic of Korea Naval Academy, Changwon
[7]School of Aerospace Engineering, Gyeongsang National University, Jinju, South Korea

*These authors contributed equally and share first authorship.

Corresponding author: Hyoung-Ho Kim, School of Aerospace Engineering, Gyeongsang National University, Jinju, 52725, South Korea. E-mail: khh106@gnu.ac.kr

Please cite this article as doi: 10.4081/jae.2026.2241

Submitted: 15 April 2026
Accepted: 23 July 2026

Optimization of microclimate uniformity in a multi-layer container-type strawberry smart farm using CFD and the Taguchi method

Min Gyu Jung,[1,2*] Md. Didarul Islam,[3*] Ji Min Jeong,[1] Byeong Jun Jeon,[4] Yong Kab Lee,[5] Min-Gyu Jeon,[6] Hyoung-Ho Kim[7]

[1]Department of Mechanical Engineering,Gyeongsang National University, Jinju
[2]Department of Horticulture; Gyeongsang National University, Jinju
[3]Graduate School of Mechanical and Aerospace Engineering, Gyeongsang National University, Jinju
[4]Jeres Farm, Yesan
[5]SIMEX Corporation, Seoul
[6]Department of Mechanical System Engineering, Republic of Korea Naval Academy, Changwon
[7]School of Aerospace Engineering, Gyeongsang National University, Jinju, South Korea

*These authors contributed equally and share first authorship.

Corresponding author: Hyoung-Ho Kim, School of Aerospace Engineering, Gyeongsang National University, Jinju, 52725, South Korea. E-mail: khh106@gnu.ac.kr

Abstract

Vertical container-type smart farms offer an effective way to improve productivity in space-limited environments, but their multi-layer arrangement often creates stagnant airflow and nonuniform microclimates. In this study, computational fluid dynamics (CFD) and the Taguchi method were combined to optimize the layout of air-conditioning components in a container-type strawberry smart farm. Three spatial design factors were considered: inlet position, outlet position, and carbon dioxide (CO_2) nozzle position. Nine cases were constructed using a three-level L9 orthogonal array, and spatial standard deviation was used as the uniformity index for temperature, CO_2 concentration, and local mean age of air (LMA). The baseline model showed low-velocity and recirculation regions around the cultivation beds and structural frame, producing substantial nonuniformity in CO_2 distribution. The middle layer had the highest mean CO_2 concentration, whereas the lower layer had the lowest concentration, with a maximum interlayer difference of 53.7 ppm. The Taguchi analysis showed that outlet position was the most influential factor, with a delta value of 8.74 and a contribution ratio of 57.78%. The optimal configuration placed the inlet at 1,200 mm, the outlet at 1,500 mm, and the CO_2 nozzle at 1,200 mm. Compared with the baseline model, this configuration reduced the standard deviation of CO_2 concentration from 75.85 to 7.08 ppm and improved the standard deviation of LMA from 5.63 to 4.98 s. However, temperature uniformity slightly decreased as the analysis used steady-state conditions, fixed operating flow rates, and a simplified crop geometry; the optimal layout should be revalidated when the container size, crop canopy density, or operating strategy changes. These results demonstrate that spatial microclimate uniformity in multi-layer container-type strawberry smart farms can be improved efficiently by optimizing component layout.

Key words: smart farm; Taguchi method; computational fluid dynamics (CFD); local mean age of air (LMA).

Introduction

Strawberry production is sensitive to the spatial uniformity of temperature, humidity, and CO_2 concentration because these environmental variables influence photosynthesis, transpiration, fruit development, yield, and fruit quality (Sun *et al.*, 2012; Miyoshi *et al.*, 2017; Ryu *et al.*, 2018; Sim *et al.*, 2020). At the same time, climate change, labor shortages, and the need for stable year-round production have increased interest in controlled-environment agriculture, plant factories, vertical farming, and smart farming systems (Benke and Tomkins, 2017; Shamshiri *et al.*, 2018; Wang *et al.*, 2023). Vertical smart farms are particularly attractive because they improve land-use efficiency by enabling multi-layer cultivation within a limited space (Banerjee and Adenaeuer, 2014; Hwang *et al.*, 2015). But enclosed and high-density structures in smart farms often restrict airflow, leading to uneven distributions of temperature, humidity, and carbon dioxide between the upper and lower cultivation layers. Liu and Song (2012) reported that vertical microclimate nonuniformity can reduce photosynthetic efficiency, cause uneven crop growth, and ultimately lower productivity. Therefore, maintaining a uniform microclimate throughout the cultivation space is essential for the successful operation of vertical smart farms, and this largely depends on the effective design of the internal air-conditioning system.

To improve the internal environment of smart farms, many studies have used computational fluid dynamics (CFD) to analyze and optimize ventilation structures. CFD is a useful method for predicting and visualizing airflow and heat transfer in complex cultivation spaces (Norton *et al.*, 2007). Previous studies have shown its value in smart farm design. Moon *et al.* (2015) arranged two sets of circulation fans at the top of a plant factory and achieved an average temperature of 296.33 K and an average airflow velocity of 0.51 m/s, while also reporting an energy-saving rate of 55.81% under optimized fan-speed conditions. In a container-type smart farm, Hwang *et al.* (2020) found that outlet position significantly affected air distribution and the local mean age of air (LMA). Zhang and Kacira (2022) compared five ventilation designs and reported that a localized ventilation system using perforated tubes installed at each cultivation shelf improved the relative standard deviations of airflow velocity, temperature, and vapor pressure deficit above the crop canopy by 14.3%, 0.1%, and 1.0%, respectively, compared with the control case. Similarly, Sohn *et al.* (2023) showed that direct air supply along the cultivation-bed length yielded an average airflow velocity of 0.65 m/s, with a coefficient of variation of 33%, whereas adding an extra outlet reduced the coefficient of variation to 10%. More recently, Chen *et al.* (2024b) compared six ventilation scenarios and reported reductions of 18.34%, 0.12%, and 2.05% in the relative standard deviations of airflow velocity, temperature, and relative humidity, respectively, compared with the control case. Their validated CFD model also showed low normalized mean-square error values for airflow velocity, temperature, and relative humidity across multiple cultivation heights, confirming its predictive reliability.

Although these studies demonstrated the usefulness of CFD for improving smart farm environments, most focused on only a limited number of design variables or compared a small number of scenarios. The internal environment of a smart farm is affected by the combined influence of multiple factors, including inlet position, outlet position, and CO_2 nozzle arrangement. Therefore, simple case-to-case comparisons are not sufficient to systematically identify the relative importance of each factor or determine the best design combination. A more efficient and quantitative optimization approach is therefore needed.

The Taguchi method provides an efficient optimization framework by using orthogonal arrays to reduce the number of required analyses while still allowing the quantitative evaluation of major design factors. In earlier CFD-based optimization research, Haghshenaskashani *et al.* (2018) demonstrated that the Taguchi method could be effectively used to identify influential design variables and determine optimal combinations with a limited number of simulations. Building on this approach, Yuce *et al.* (2022) further showed that Taguchi-based CFD analysis is useful for evaluating ventilation performance and reducing computational cost in thermal and airflow-related problems. More recently, Park *et al.* (2023) applied CFD with an L9 orthogonal array to optimize the outlet shape of an air-circulation system in a smart farm, reducing the time required to alleviate vertical temperature differences from 820 s to 90 s. Subsequently, Chen *et al.* (2024a) extended this concept to an indoor vertical farming system by combining inverse CFD with the Taguchi method to analyze ventilation characteristics.

Accordingly, the present study used an L9 orthogonal array to efficiently evaluate three design factors at three levels each. The inlet position, outlet position, and CO_2 nozzle position were selected as the main design factors because they are layout variables that can be modified during construction or retrofitting without increasing the continuous operating energy demand. Increasing fan speed or changing the fan type can also improve mixing, but such control-based strategies generally require higher power consumption and may introduce excessive local air velocity around the crop canopy. Recent plant-factory airflow studies have reported that excessive air change rate or excessive inflow velocity can cause canopy-level air velocity to deviate from the optimal range and may negatively affect photosynthesis and transpiration behavior (Gu and Goto, 2024a; Gao *et al.*, 2025). By contrast, optimizing the geometric arrangement of air-supply, exhaust, and CO_2-injection components can improve the pressure field, circulation path, and gas distribution using the existing air-conditioning capacity. The Taguchi method was therefore adopted to evaluate these coupled layout effects efficiently and to identify the relative importance of each factor without performing all 27 full-factorial CFD simulations. The objectives of this study were to: (1) establish a measurement-based CFD model of a multi-layer container-type strawberry smart farm; (2) quantify how inlet position, outlet position, and CO_2 nozzle position affect the spatial standard deviations of temperature, CO_2 concentration, and LMA; and (3) identify and verify an optimal air-conditioning layout using S/N ratio analysis and ANOVA within a Taguchi L9 orthogonal-array framework.

Methodology

Modelling of smart farm

This study was conducted using the measured dimensions of a container-type smart farm located in Yesan-gun, Chungcheongnam-do, Republic of Korea. Photographs of the exterior facility and internal cultivation system are provided in the Supplementary Material (Figure S1). To reduce computational cost, fine crop features such as individual leaves and stems were simplified. Nevertheless, the positions of the cultivation beds and the major structural dimensions were preserved to construct the three-dimensional geometric model shown in Figure 1. Accordingly, canopy resistance coefficients, crop transpiration, and crop sensible heat exchange were not included in the present steady-state simulations. The model was therefore intended to evaluate the influence of air-conditioning component layout on room-scale distributions of temperature, CO_2 concentration, and LMA, rather than microscale leaf-boundary-layer transport.

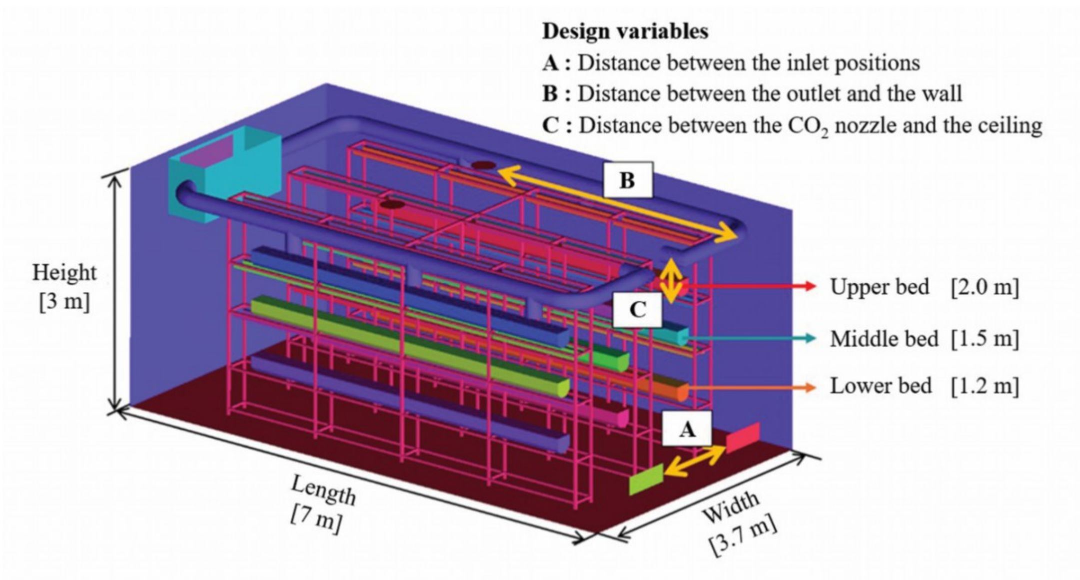

Figure 1. Dimensions of the smart farm and design parameters used for optimization.

Three design factors were selected for optimization: inlet position (A), outlet position (B), and CO_2 nozzle position (C). The inlet position directly influences the formation and circulation path of the main internal airflow, whereas the outlet and CO_2 nozzle positions affect the diffusion and mixing behavior of the supplied CO_2 , and the location of each design factor was defined as the distance from the reference point.

Computational setup for numerical analysis

Mesh generation and grid independence

The computational mesh was generated using ANSYS ICEM and consisted of a tetrahedron-based hybrid grid. Figure 2 illustrates the mesh configuration adopted in this study. Figure 2a presents the surface mesh of the entire computational domain, and Figure 2b shows the mesh distribution in an internal cross-section. Mesh refinement was applied near the cultivation beds and around the inlet and outlet regions, where large gradients in airflow and heat transfer and species transport were expected. Three mesh levels were tested to verify that the selected grid density provided sufficient numerical accuracy for the outlet mass-flow response used in the grid-independence evaluation.

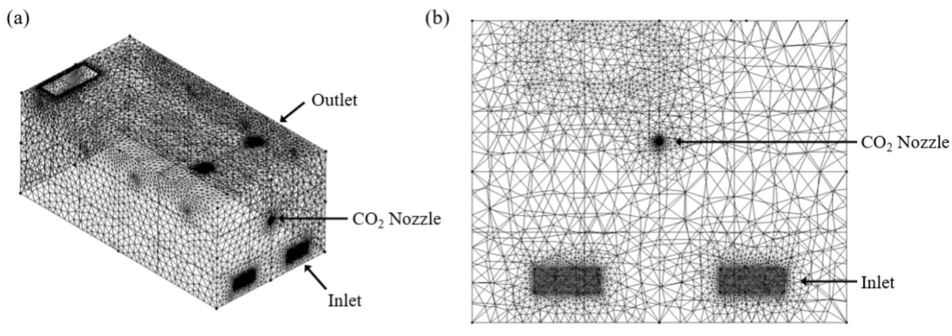

Figure **2.** Mesh configuration of the smart farm computational domain. **a)** Overall grid configuration; **b)** cross-sectional view.

To assess the reliability of the numerical results and quantify mesh-related numerical uncertainty, a grid-dependence test was performed using the grid convergence index

(GCI). The GCI evaluates grid independence based on differences in numerical results obtained from multiple mesh levels and was calculated using Eqs. (1) and (2).

$$e_a = \left|\frac{\phi_{new} - \phi_{old}}{\phi_{new}}\right| \times 100\% \qquad \text{(Eq. 1)}$$

$$GCI = \frac{1.25 \times e_a}{r^p - 1} \qquad \text{(Eq. 2)}$$

Here, ϕ_{old} and ϕ_{new} denote the outlet mass flow rates obtained from the baseline and refined meshes, respectively, r presents the grid refinement ratio, p is the apparent order of accuracy, and e_a is the approximate relative error.

As summarized in Table 1, the outlet mass flow rate was monitored for coarse, medium, and fine mesh levels. The fine mesh contained approximately 3.32×10^7 elements and produced a GCI value of 4.25%. As this value was below the commonly used 5% grid-convergence criterion, the fine mesh was selected for the present simulations without sacrificing numerical reliability.

Table 1. GCI results for the smart farm CFD model.

Parameters	**Values**
Mesh: Fine / Medium / Coarse ($\mathbf{N}_1$ / $\mathbf{N}_2$ / $\mathbf{N}_3$)	Elements: (3.32×10^7 / 2.79×10^7 / 1.18×10^7)
Grid refinement ratio, $\boldsymbol{r}_{21}$	1.06
Grid refinement ratio, $\boldsymbol{r}_{32}$	1.33
Outlet mass flow rate for fine mesh, ϕ_1	46.236×10^{-5} (kg/s)
Outlet mass flow rate for medium mesh, ϕ_2	46.256×10^{-5} (kg/s)
Outlet mass flow rate for coarse mesh, ϕ_3	47.798×10^{-5} (kg/s)
Apparent order, p	2.00
Extrapolated mass flow rate, ϕ_{ext}^{31}	44.664×10^{-5} (kg/s)
Approximate relative error, $\mathbf{e}_a^{31}$	3.38%
Approximate relative error, $\mathbf{e}_{ext}^{31}$	3.51%
Grid Convergence Index, $\mathbf{GCI}_{fine}^{3}$	4.25%

Numerical setup, boundary conditions, and canopy treatment

ANSYS CFX 2020 R1 was used to analyze airflow, heat transfer, and CO_2 concentration distributions inside the smart farm. Fluid behavior was described using the continuity equation for mass conservation and the momentum equation, given in Eqs. (3) and (4).

$$\frac{\partial u_j}{\partial x_j} = 0 \qquad \text{(Eq. 3)}$$

$$\frac{\partial \left(\rho u_i u_j\right)}{\partial x_j} = -\frac{\partial p}{\partial x_i} + \frac{\partial \tau_{ij}}{\partial x_j} + S_i \qquad \text{(Eq. 4)}$$

In Eq. (3), ρ denotes fluid density, u_j is the velocity component, and x_j is the spatial coordinate. In Eq. (4), p denotes pressure, τ_{ij} is the viscous stress tensor, and S_i represents the body force. In this study, buoyancy induced by gravity and density variation was incorporated into the body-force term to account for natural convection arising from temperature and CO_2 concentration differences inside the container-type smart farm. For turbulence modeling, the Shear Stress Transport (SST) model was adopted. This model combines the advantages of the $k-\varepsilon$ and $k-\omega$ formulations by applying the $k-\omega$ model near the wall and the $k-\varepsilon$ model in the outer flow region. It is therefore well-suited for complex flow fields involving adverse pressure gradients (Menter, 1994).

Although the operating conditions of an actual smart farm vary with the day-night cycle, the present study assumed steady environmental conditions during the period from 5:00 a.m. to 8:30 a.m., when crop physiological activity and air-conditioning control are most active. Accordingly, steady-state simulations were performed. A high-resolution scheme was used for spatial discretization, and the continuity and momentum equations were solved simultaneously using a pressure-based coupled solver. Convergence was assumed when the root mean square (RMS) residual of each governing equation was less than 10^{-5}. Ventilation performance was quantitatively evaluated using LMA, which represents the average residence time required for incoming air to reach a given location after entering the computational domain. Lower LMA values indicate faster air renewal and better ventilation performance.

The working fluid was modeled as an ideal gas mixture of dry air, water vapor, and CO_2. The thermophysical properties of each component are listed in Table 2. Boundary conditions for the computational domain were established using measurements obtained from the actual smart farm. Detailed measurement data and sensor locations used to define these conditions are provided in Figure S2 of the Supplementary Material.

Table 2. Thermophysical properties of the working fluids.

	Molar mass (g/mol)	Density (kg/m^3)	Specific heat capacity (J/kg K)	Thermal expansivity (1/K)
Dry air	28.9647	1.257	1.005 $\times 10^3$	3.596 $\times 10^{-3}$
Water vapor	18.01	7.725 $\times 10^{-3}$	1,860	3.569 $\times 10^{-3}$
CO_2	44.01	1.977	851	3.66 $\times 10^{-3}$

The inlet, outlet, and air-conditioning-related boundary conditions were fixed using the measured operating values. Only the positions of the inlet, outlet, and CO_2 nozzle were changed, as these were the design variables considered in this study. The principal boundary conditions and modeling assumptions are summarized in Table 3.

Table 3. Boundary and modeling conditions used in the CFD simulations.

Parameter	Value / Condition
Analysis type	Steady-state simulation during 5:00 a.m. ~ 8:30 a.m.
Working fluid	Ideal gas mixture of dry air, water vapor, and CO_2
Turbulence model	Shear Stress Transport (SST) model
Inlet air condition	Measured inlet air mass flow rate: 0.3549 kg/s (fixed in all cases)
Outlet condition	Fixed outlet boundary; only outlet position was varied among Taguchi cases
CO_2 nozzle supply	Pure CO_2; nozzle mass fraction = 1.0
CO_2 mass flow rate	0.27 g/s (fixed in all cases)
Target / initial CO_2 mass fraction	0.00137 / 0.00061
Relative humidity (RH)	70%
Wall /duct temperature	17 °C / 21 °C
LED cover / LED temperature	35 °C / 38 °C
Crop canopy treatment	Cultivation beds and major structures retained; individual leaves and stems simplified; no porous canopy resistance, transpiration, or crop sensible heat source included

The inlet boundary was therefore specified by the measured mass flow rate rather than by a prescribed inlet velocity. This choice was made to keep the operating air-conditioning capacity identical across all design cases and to isolate the effect of component location on the internal flow and scalar fields.

The CO_2 supply conditions were identically applied to all design cases based on actual operating settings. The CO_2 mass fraction and required supply flow rate were calculated using Eqs. (5) and (6).

$$Y_{CO_2} = \frac{\chi_{CO_2} M_{CO_2}}{\chi_{CO_2} M_{CO_2} + \chi_{vapor} M_{vapor} + \chi_{air} M_{air}} \quad \text{(Eq. 5)}$$

$$\dot{m}_{CO_2} = \frac{Y_t - Y_0}{1 - Y_t} \dot{m}_{air} \quad \text{(Eq. 6)}$$

In Eq. (5), χ_i denotes mole fraction and M_i denotes molar mass. In Eq. (6), Y_t is the target CO_2 mass fraction, set to 0.00137, and Y_0 is the initial atmospheric CO_2 mass fraction, set to 0.00061. The measured inlet air mass flow rate, $\dot{m}_{air}$, was 0.3549 kg/s and was held constant for all cases. Because liquefied CO_2 is supplied from a high-pressure tank in the actual facility, the gas introduced through the nozzle was assumed to be pure CO_2 without impurities. Accordingly, the CO_2 mass fraction at the nozzle inlet boundary was set to 1.0.

Based on Eqs. (5) and (6), the CO_2 mass flow rate was calculated as 0.27 g/s, and this value was applied in all cases. The LED lighting system, which served as an internal heat source, was modeled using measured wall temperatures of 38°C for the light-emitting section and 35°C for the cover. This allowed the effect of LED heat generation on internal temperature distribution to be included in the simulations.

Process of design analysis using the Taguchi method

Evaluation metrics

To quantify spatial microclimate nonuniformity from the CFD results, spatial standard deviation was used as the uniformity index. The arrangement of air-conditioning components that minimized this index was identified using the Taguchi method. All statistical analyses and visualizations were performed using Minitab 22 software (Minitab Inc., USA). Through the Taguchi design of experiments, the major factors affecting spatial standard deviation were identified. Signal-to-noise (S/N) ratio analysis was then used to minimize spatial nonuniformity and determine the factor-level combination that yielded the most favorable internal cultivation environment.

Optimization design process

The procedure begins with model preparation and the definition of performance objectives, followed by the selection of design factors and levels, as shown in the flow chart in Figure 3.

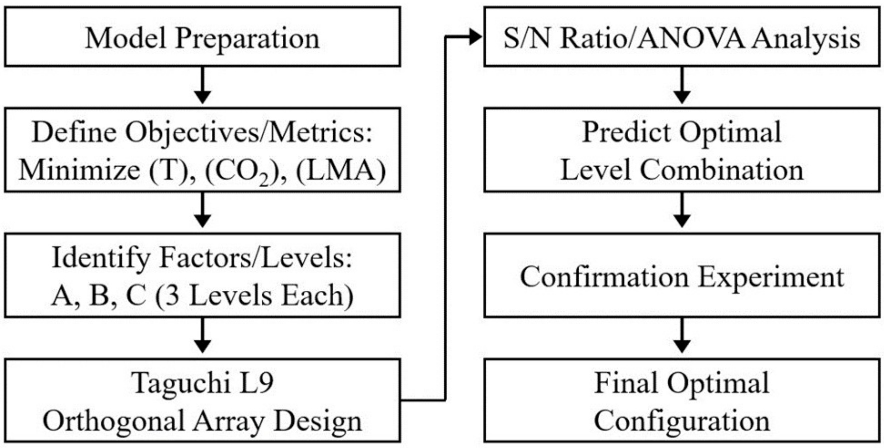

Figure 3. Overall workflow of the optimization process.

A Taguchi L9 orthogonal array is then used to plan the experiments efficiently. The results are evaluated through S/N ratio and ANOVA analyses to predict the optimal factor combination, which is finally verified through a confirmation experiment. The major design factors affecting the spatial uniformity of the internal smart farm environment were selected as inlet position (A), outlet position (B), and CO_2 nozzle position (C). The level values for each factor were determined based on the feasible installation range and structural constraints of the actual container-type smart farm. The inlet and CO_2 nozzle positions were assigned three levels of 0, 1,200, and 2,400 mm from the reference point shown in Figure 1, representing low, intermediate, and high positions within the practical installation range. The outlet position was assigned three levels of 1,500, 3,500, and 5,500 mm, considering the ceiling structure and internal equipment layout. The definitions and levels of the design factors are listed in Table 4.

Table 4. Control factors and their levels.

Symbol	Factor	Unit	Level 1	Level 2	Level 3
A	Inlet position	mm	0	1,200	2,400
B	Outlet position	mm	1,500	3,500	5,500
C	CO_2 nozzle position	mm	0	1,200	2,400

Based on these factor-level combinations, the Taguchi L9 orthogonal array shown in Table 5 was employed.

Table 5. Experimental layout based on the Taguchi L9 orthogonal array.

Exp. no.	Inlet (mm)	Outlet (mm)	CO_2 Nozzle (mm)
1	0	1,500	0
2	0	3,500	1,200
3	0	5,500	2,400
4	1,200	1,500	1,200
5	1,200	3,500	2,400
6	1,200	5,500	0
7	2,400	1,500	2,400
8	2,400	3,500	0
9	2,400	5,500	1,200

This design enables the main effects of three factors at three levels each to be evaluated using nine representative combinations instead of all 27 possible full-factorial combinations. Accordingly, a total of nine CFD cases were constructed.

To quantify the effect of each factor on the performance index, S/N ratio analysis was performed. Because lower environmental deviation corresponds to better spatial uniformity, the smaller-the-better criterion was used, as expressed in Eq. (7).

$$S/N = -10\log_{10}\left(\frac{1}{n}\sum_{i=1}^{n} y_i^2\right) \qquad \text{(Eq. 7)}$$

Here, *S/N* denotes the signal-to-noise ratio, *n* is the number of experiments, and y_i is the observed spatial standard deviation of the response variable. A larger *S/N* ratio, therefore, indicates a lower deviation and a more uniform cultivation environment.

Results

Optimized configuration by Taguchi analysis

The relative influence of the design factors on spatial nonuniformity within the smart farm was evaluated using the S/N ratios shown in Figure 4.

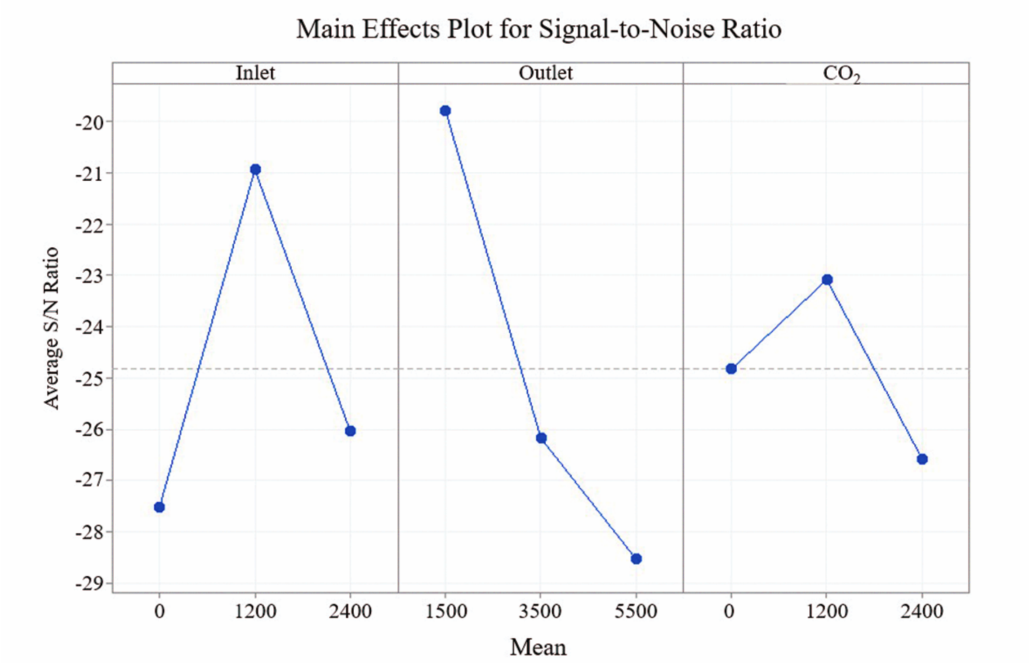

Figure 4. Main effects plots for the S/N ratio.

The outlet position exhibited the steepest slope across its levels, indicating the greatest variation in S/N ratio with changes in factor level. In contrast, the inlet position showed a more moderate effect, while the CO_2 nozzle position produced the smallest variation. Under the smaller-the-better criterion, the level associated with the highest S/N ratio was selected as the optimal condition. Based on the main effects plot, the optimal factor-level combination was determined to be an inlet position of 1,200 mm, an outlet position of 1,500 mm, and a CO_2 nozzle position of 1,200 mm.

The ANOVA results presented in Table 6 support the same trend. All three design factors significantly affected the S/N ratio ($p < 0.01$). Among them, the outlet position (B) showed the largest F-value (990.73) and the highest contribution ratio (57.78%), confirming that it was the dominant factor governing environmental uniformity inside the smart farm. The inlet position (A) was the second most influential factor, with a contribution ratio of 33.56%, followed by the CO_2 nozzle position (C) with 8.61%. The residual error was only 0.06%, indicating that the selected design factors and experimental setup explained nearly all the variation in the S/N ratio.

Overall, the Taguchi analysis clearly identified the outlet position as the most critical design variable affecting spatial uniformity. The optimal combination obtained from this analysis was therefore adopted to define the optimized model (OM), which was subsequently compared with the baseline model (BM) in terms of airflow renewal, temperature distribution, and CO_2 uniformity.

Table 6. ANOVA results for S/N ratios**.**

Source	**DF**	**Seq SS**	**Adj MS**	**F-value**	***p*-value**	**Contribution (%)**
Inlet (A)	2	71.288	35.6440	575.37	0.002	33.56
Outlet (B)	2	122.751	61.3754	990.73	0.001	57.78
CO_2 nozzle (C)	2	18.284	9.1420	147.57	0.007	8.61
Residual error	2	0.124	0.0619	-	-	0.06
Total	8	212.447	-	-	-	100.0

Analysis of the smart farm models (BM *vs* OM)

We compare the baseline model (BM) and the optimized model (OM) in terms of airflow renewal and microclimate uniformity within the smart farm. The analysis is organized in two steps. First, the air flow behavior is evaluated using the LMA, which reflects the air-renewal performance within the cultivation space. Second, the temperature and CO_2 distributions in the strawberry bed areas are examined to assess how the modified airflow structure influenced the local growing environment. For consistency, the cultivation layers are described here as the upper, middle, and lower bed areas.

LMA analysis of full smart farm areas (BM vs OM)

Figure 5 presents the LMA contours overlaid with velocity vectors for the BM and OM. In the BM, Figure 5a, the supplied air followed a relatively limited internal path, and low-LMA regions were confined to narrow flow routes. In contrast, broad high-LMA regions developed around the multilayer cultivation beds, frame structures, and near the walls and corner regions, where the velocity vectors weakened. Because high LMA indicates slow arrival of fresh air, these results suggest insufficient air exchange and the formation of stagnant zones inside the cultivation space. Such stagnation is likely to promote spatial nonuniformity in temperature, CO_2, and humidity-related transport. In the OM, Figure 5b, the rearranged inlet, outlet, and CO_2 nozzle produced a more continuous airflow path through the cultivation zone. Compared with the BM, the high-LMA regions associated with wake zones behind structures and with the lower part of the domain were clearly reduced. This indicates that the optimized layout improved the overall air-renewal performance of the smart farm by weakening stagnant regions and promoting more effective internal mixing.

LMA analysis of strawberry bed areas (BM vs OM)

The LMA distributions within the strawberry bed areas are shown in Figure 6. In the BM as shown in Figure 6a, relatively high LMA values were observed in regions shielded by internal structures and in low-velocity zones, indicating weak local air renewal in the crop-growing region. In the OM as shown in Figure 6(b), the LMA distribution became more balanced across the cultivation layers. In the BM, the mean LMA was highest in the middle bed (31.33±4.60 s), followed by the upper bed (30.67±4.75 s), whereas the lower bed had a lower mean value but the largest variation (26.63±7.97 s). This large variation implies that well-ventilated and poorly ventilated regions coexisted within the same lower cultivation layer. In the OM, the LMA distribution became more balanced across the cultivation layers. The mean LMA values were 26.81±6.49 s in the upper bed, 27.17±6.01 s in the middle bed, and 28.1 ±4.43 s in the lower bed, giving a maximum interlayer difference of only 1.36 s. More importantly, the LMA standard deviation in the lower bed decreased from 7.97 s in the BM to 4.43 s in the OM. Overall, the standard deviation of LMA decreased from 5.63 s to 4.98 s after optimization. These results indicate that the optimized configuration improved the spatial uniformity of air renewal, especially in the lower cultivation region, where nonuniformity was most evident in the BM.

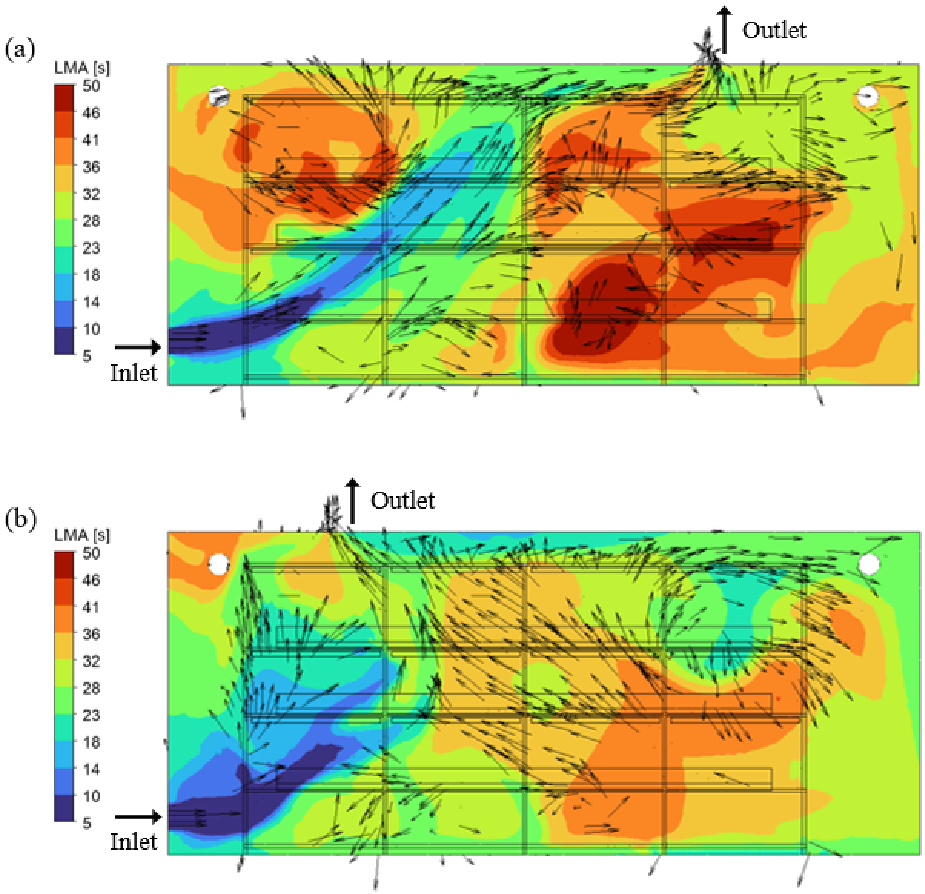

Figure 5. LMA contours overlaid with velocity vectors of BM **(a)** and OM **(b)**.

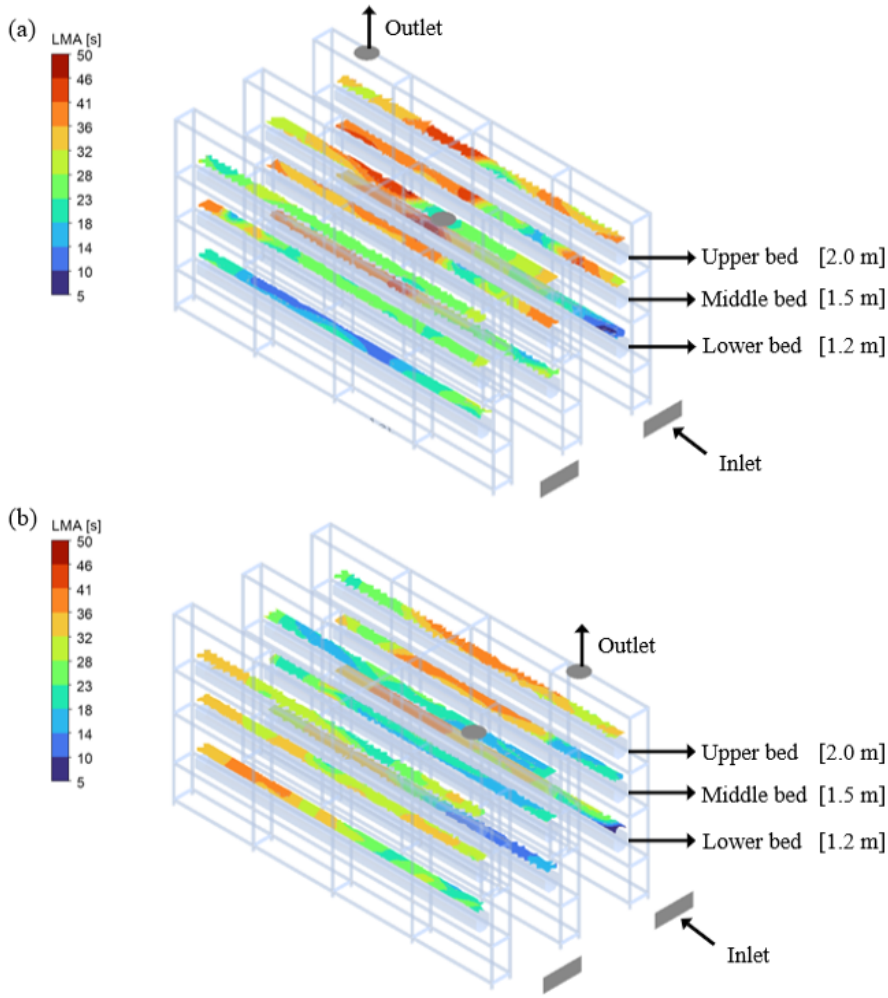

Figure 6. LMA distributions within the strawberry bed areas BM **(a)** and OM **(b)**.

Analysis of the temperature and CO_2 distribution on the strawberry bed areas (BM *vs* OM)

Temperature distribution on the strawberry bed areas (BM vs OM)

The temperature distributions in the strawberry bed areas for the BM and OM are shown in Figure 7. In the BM as shown in Figure 7a, the temperature field was generally smooth throughout the cultivation zone, although localized temperature differences were still observed in several regions.

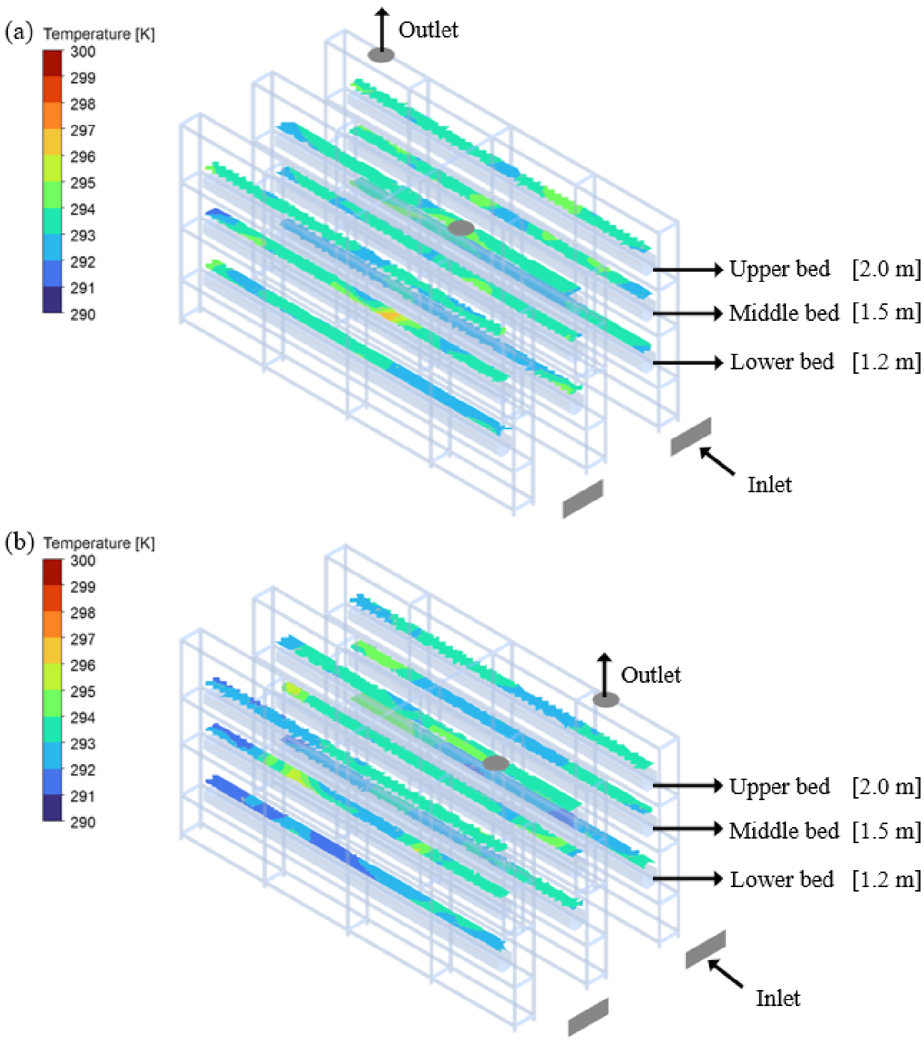

Figure 7. Temperature within the strawberry bed areas: BM **(a)** and OM **(b)**..

On the contrary, as shown in Figure 7b, the temperature field remained broadly stable, but stronger local variations appeared in some cultivation areas. In the BM, the middle bed had the highest mean temperature (20.25±0.10°C), followed by the upper bed (20.12±0.15°C), while the lower bed had the lowest mean temperature (19.82±0.23°C). The maximum interlayer temperature difference in the BM was therefore approximately 0.43°C, indicating a modest but measurable vertical temperature gradient within the baseline layout. For the OM, the upper, middle, and lower beds showed mean temperatures of 19.98±0.25°C, 20.08±0.15°C, and 19.48±0.38°C, respectively. Thus, the middle bed still had the highest mean temperature, whereas the lower bed had the lowest mean temperature and the largest standard deviation. The maximum interlayer temperature difference increased to approximately 0.60°C after optimization.

CO_2 Distribution on the strawberry bed areas (BM vs OM)

A clear difference in CO_2 distribution between BM and OM is shown in Figure 8. In the BM, as shown in Figure 8(a), localized high-CO_2 regions developed in parts of the cultivation area, while other zones maintained relatively lower concentrations, indicating pronounced spatial deviation.

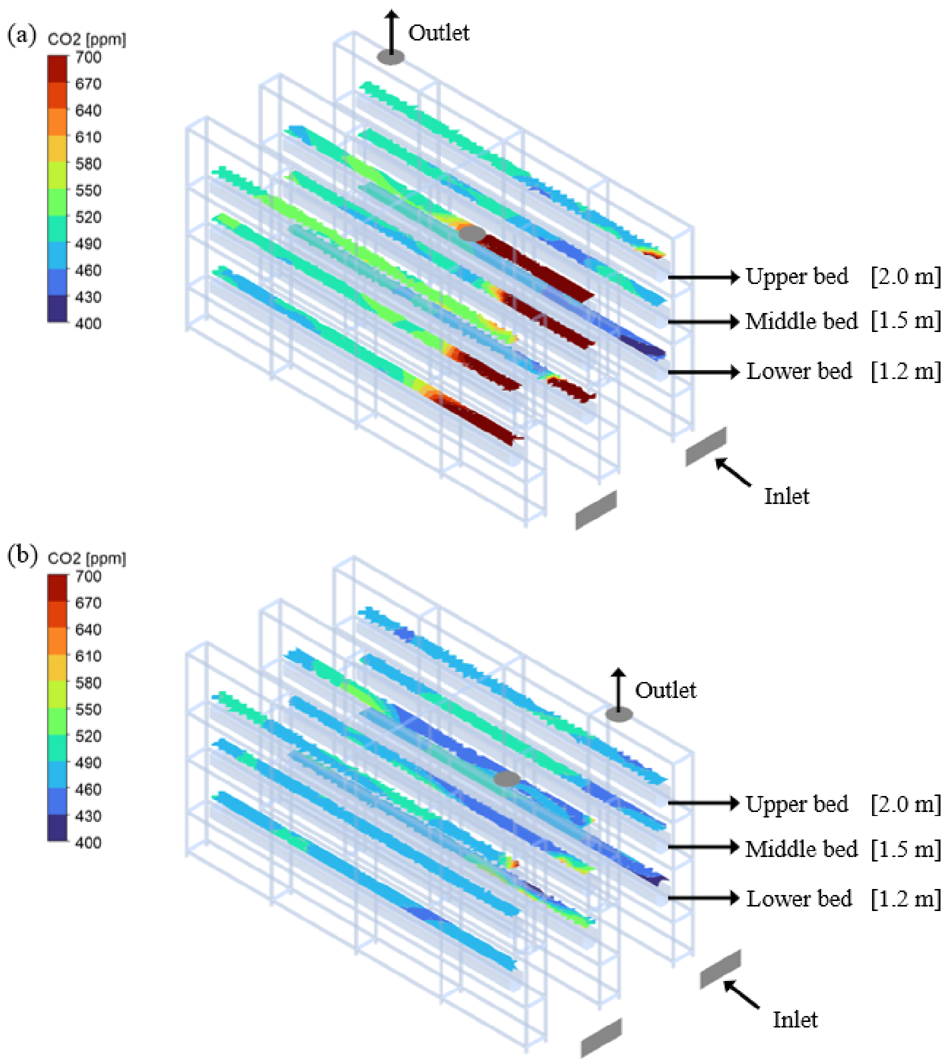

Figure 8. CO_2 in the strawberry bed areas: BM **(a)** and OM **(b)**.

On the other hand, for OM as of Figure 8b, the CO_2 field became markedly more uniform throughout the strawberry bed areas. The middle bed had the highest mean CO_2 concentration (587.93±111.82 ppm), followed by the upper bed (557.27±72.59 ppm), while the lower bed had the lowest value (534.23±55.32 ppm).

The maximum interlayer difference was 53.70 ppm, and the middle bed also exhibited the largest within-layer standard deviation, suggesting strong coexistence of local accumulation and dilution within the same cultivation layer. By contrast, in the OM, the CO2 field became markedly more uniform throughout the strawberry bed areas, with mean concentrations of 478.77±9.96 ppm in the upper bed, 477.37±8.27 ppm in the middle bed, and 478.13 ± 5.65 ppm in the lower bed.

The maximum interlayer difference was only 1.40 ppm. These results demonstrate that the optimized layout effectively suppressed local CO_2 accumulation and promoted more uniform gas mixing throughout the cultivation space.

Discussion

This study addressed the recurring issue of layer-wise microclimate nonuniformity in a container-type vertical strawberry smart farm by optimizing the arrangement of air-conditioning components through a combined CFD-Taguchi approach. In the BM, the multi-layer cultivation beds and structural frame increased airflow resistance, and air exchange became concentrated along limited flow paths. As a result, stagnant regions with high LMA and localized CO_2 accumulation developed within the cultivation space. This behavior is consistent with previous studies reporting that temperature, humidity, and CO_2 gradients develop along airflow paths in controlled cultivation environments (Teitel *et al.*, 2010; Jerszurki *et al.*, 2021). Hwang *et al.* (2020) similarly reported that inlet position and ventilation path strongly influence LMA and environmental uniformity in a container-type smart farm. Studies of indoor plant factories and shipping-container vertical farms have likewise shown that inlet-outlet arrangement and air-distribution strategy govern canopy-level airflow and microclimate uniformity (Sohn *et al.*, 2023; Zhang and Kacira, 2022). Accordingly, the middle-layer CO_2 accumulation and lower-layer stagnation observed in BM should not be regarded as system-specific anomaliesbut rather as typical manifestations of microclimate nonuniformity resulting from the interaction between vertical cultivation structures and suboptimal air distribution.

The Taguchi analysis identified outlet position as the most influential design factor. Physically, this can be explained by the outlet reorganizing the pressure field and streamline structure throughout the domain, thereby simultaneously controlling the primary circulation pattern, removing stagnant air and the diffusion path of CO_2. Sohn *et al.* (2023) reported that outlet configuration significantly affects canopy-level airflow uniformity in a shipping-container vertical farm, whereas Chen *et al.* (2024b) emphasized that an appropriate airflow pattern is essential for maintaining environmental uniformity in a micro-plant factory. When the outlet is in a position that draws air through the cultivation layers, a stronger pressure-gradient path is formed across the multi-layer trays, reducing wake zones behind the frame and improving gas exchange around the beds. Conversely, an outlet position that extracts air too early along the ceiling or side-wall path can promote short-circuiting, in which part of the supplied air leaves the domain before sufficiently sweeping the crop-growing region. This explains why the outlet location affected microclimate uniformity more strongly than the CO_2 injection point itself: the nozzle position controls the source location of CO_2, whereas the outlet position controls the bulk transport pathway that distributes or removes the supplied scalar throughout the entire container. Kang and van Hooff (2024) also showed that the design of the air distribution system strongly affects both air distribution and excess heat removal in a compact vertical farm. The effect shows that outlet configuration and airflow pattern strongly influence canopy-level airflow and environmental uniformity in container-type and compact vertical farms.

In the OM obtained from the confirmation analysis, the primary circulation airflow passed through the cultivation space more continuously than in the BM, and the wake regions behind structures, together with the low-velocity zones in the lower part of the domain, were alleviated. This result agrees with previous reports showing that improved air distribution enhances airflow and microclimate uniformity around the crop canopy. Zhang *et al.* (2016) demonstrated that perforated air tubes can improve airflow uniformity in indoor plant factories, while Fang *et al.* (2020) reported that improper ventilation design may induce stagnation in the canopy boundary layer when crop resistance and LED heat dissipation are considered. Ahmed *et al.* (2020) suggested that multi-fan systems improve air flow around crops and may support growth while reducing tip-burn risk. More recently, Agati *et al.* (2024) and Gu and Goto (2024a, 2024b) demonstrated, using sensor-validated CFD models and realistic plant structures, that airflow conditions directly influence temperature, humidity, and air distribution near the canopy. From this perspective, the marked reduction in CO_2 standard deviation together with the improvement in LMA uniformity observed in the OM should be interpreted as evidence of genuinely improved overall microclimate uniformity through reduced stagnant zones and enhanced mixing, rather than simply as a shift in mean values.

By contrast, the temperature standard deviation increased relative to that of the BM, indicating a possible trade-off between improved CO_2 diffusion and air-renewal performance on the one hand, and thermal uniformity on the other. This suggests that modifications to the airflow path can affect local convective heat-transfer behavior differently from gas mixing. Previous studies have similarly shown that temperature and humidity fields in vertical farming systems are sensitive to airflow structure and inflow conditions (Agati *et al.*, 2024; Chen *et al.*, 2024b; Gu and Goto, 2024a, 2024b; Kang and van Hooff, 2024). Therefore, the increase in temperature deviation observed here should not be interpreted as anomalous, but rather as a plausible consequence of single-objective optimization that prioritized CO_2 and LMA uniformity. Future work should therefore consider multi-objective optimization strategies that simultaneously account for supply-air temperature, flow rate, diffuser geometry, and auxiliary circulation fans.

It should also be emphasized that the optimization performed in this study was directed toward improving spatial uniformity rather than achieving a target mean CO_2 concentration, since both the CO_2 supply rate and the air-conditioning operating conditions were fixed. In strawberry cultivation, however, both the mean CO_2 level and its spatial uniformity are important. Previous studies have shown that CO_2 enrichment can improve photosynthesis, assimilate distribution, and yield (Tagawa *et al.*, 2022), while localized CO_2 supply near the canopy can enhance yield and energy-use efficiency in strawberry production systems (Hidaka *et al.*, 2022; Miyoshi *et al.*, 2017; Mochizuki *et al.*, 2022; Zhang *et al.*, 2022). In addition, Shin *et al.* (2024) demonstrated that CO_2 concentration in strawberry greenhouses changes substantially over time, emphasizing the importance of prediction and control. Therefore, although the optimal layout identified in this study is meaningful in reducing spatial CO_2 deviation, maximizing actual crop productivity will require integrated design-and-operation optimization that simultaneously considers the mean concentration set point, injection timing, and a ventilation-coupled control strategy.

Finally, the methodological contribution of this study lies in the fact that the influence of major design factors in a container-type vertical smart farm was quantitatively evaluated, and a practical optimal layout was derived using only a limited number of simulations through the L9 orthogonal array. This is consistent with previous studies reporting that Taguchi-based CFD optimization is effective for ventilation and indoor environmental design problems (Haghshenaskashani *et al.*, 2018; Yuce *et al.*, 2022). Nevertheless, several limitations should be acknowledged. The present analysis was based on steady-state simulations and simplified crop geometry, and did not fully account for diurnal operating changes, crop-canopy resistance and transpiration, or the time-dependent variation of humidity and vapor pressure deficit observed in practice. Future work should therefore incorporate additional sensor-based validation, transient analysis, more advanced canopy modeling, and multi-objective optimization that simultaneously considers temperature, CO_2, and LMA.

Conclusions

In this study, the air-conditioning layout of a container-type vertical strawberry smart farm was optimized by integrating CFD with the Taguchi method to reduce spatial microclimate nonuniformity within the cultivation space. The main findings are summarized as follows.

a. The baseline model showed that the multi-layer cultivation structure and supporting frame increased airflow resistance and generated low-velocity and recirculation zones, thereby amplifying the spatial nonuniformity of CO_2 concentration and LMA. The mean CO_2 concentrations were 557.27 ppm in the upper layer, 587.93 ppm in the middle layer, and 534.23 ppm in the lower layer. The maximum interlayer difference was 53.7 ppm between the middle and lower layers, confirming the presence of pronounced layer-wise microclimate deviation.

b. Based on S/N ratio analysis and ANOVA using the Taguchi L9 orthogonal array, outlet position was identified as the dominant factor affecting environmental deviation, with a contribution ratio of 57.78%, followed by inlet position at 33.56% and CO_2 nozzle position at 8.61%. The optimal factor-level combination was determined to be an inlet at 1,200 mm, an outlet at 1,500 mm, and a CO_2 nozzle at 1,200 mm.
c. The optimized model derived from the confirmation analysis produced a flow field with reduced stagnant zones and enhanced mixing relative to the baseline model. As a result, the standard deviation of CO_2 concentration decreased from 75.85 ppm to 7.08 ppm, corresponding to a reduction of approximately 90.7%, while the standard deviation of LMA improved from 5.63 s to 4.98 s, corresponding to an improvement of approximately 11.5%. In contrast, the temperature standard deviation increased from 0.242°C to 0.367°C, suggesting a possible trade-off among gas diffusion, ventilation performance and thermal uniformity.
d. Overall, the results demonstrate that outlet position is a key design factor governing microclimate uniformity in a container-type vertical smart farm and confirm the effectiveness of the integrated Taguchi-CFD approach for deriving an optimal design with a limited number of simulations. For smart farm builders and commercial operators, the findings suggest that outlet placement should be considered at the early design stage, because a properly located exhaust path can reduce stagnant zones and improve CO_2 uniformity without relying only on higher fan speed or additional operating energy. However, the recommended configuration was obtained for the present container geometry, fixed flow rate, fixed CO_2 supply condition, and simplified canopy representation. Therefore, the optimum should be revalidated if the container length, number of cultivation layers, outlet hardware, strawberry cultivar, or canopy density changes substantially. In future work, the practical applicability and robustness of the approach should be improved by optimizing the supply flow rate and control strategies to target the CO_2 concentration, enhancing the model to account for humidity and crop-canopy effects, and employing multi-objective optimization that simultaneously considers temperature, CO_2, and LMA.

References

Agati G, Franchetti B, Rispoli F, Venturini P, 2024. Thermo-fluid dynamic analysis of the air flow inside an indoor vertical farming system. Appl Therm Eng 236:121553.

Ahmed HA, Yu-Xin T, Qi-Chang Y, 2020. Lettuce plant growth and tipburn occurrence as affected by airflow using a multi-fan system in a plant factory with artificial light. J Therm Biol 88:102496.

Banerjee C, Adenaeuer L, 2014. Up, up and away! The economics of vertical farming. J Agric Stud 2:40.

Benke K, Tomkins B, 2017. Future food-production systems: vertical farming and controlled-environment agriculture. Sustain Sci Pract Policy 13:13-26.

Chen HT, Huang YC, Rashidi S, Chen BL, Yan WM, 2024a. Numerical and experimental studies on heat transfer characteristics and ventilation for indoor vertical farming system. Therm Sci Eng Prog 52:102667.

Chen X, Hou T, Liu S, Guo Y, Hu J, Xu G, Ma G, Liu W, 2024b. Design of a micro-plant factory using a validated CFD model. Agriculture 14:2227.

Fang H, Li K, Wu G, Cheng R, Zhang Y, Yang Q, 2020. A CFD analysis on improving lettuce canopy airflow distribution in a plant factory considering the crop resistance and LEDs heat dissipation. Biosyst Eng 200:1-12.

Gao H, Tan ZC, Yang M, Ma CP, Tang YF, Zhao FY, 2025. Microclimate air motion and uniformity of indoor plant factory system: effects of crop planting density and air change rate. Appl Sci 15:4329.

Gu X, Goto E, 2024a. Computational fluid dynamics model with realistic plant structures to study airflow in and around a plant canopy on a cultivation shelf in a plant factory with artificial light. Agriculture 14:1199.

Gu X, Goto E, 2024b. Evaluation of plant canopy microclimates with realistic plants in plant factories with artificial light using a computational fluid dynamics model. Build Environ 264:111876.

Haghshenaskashani S, Sajadi B, Cehlin M, 2018. Multi-objective optimization of impinging jet ventilation systems: Taguchi-based CFD method. Build Simul 11:1207-1214.

Hidaka K, Nakahara S, Yasutake D, Zhang Y, Okayasu T, Dan K, Kitano M, Sone K, 2022. Crop-local CO2 enrichment improves strawberry yield and fuel use efficiency in protected cultivations. Sci Hortic 301:111104.

Hwang HS, Lee SH, Han SH, 2020. Estimation of ventilation efficiency to improve growing conditions in container smart farms. Trans Korean Soc Mech Eng A 44:873-879.

Hwang SI, Joo JM, Joo SY, 2015. ICT-based smart farm factory systems through the case of hydroponic ginseng plant factory. J Korean Inst Commun Inf Sci 40:780-790.

Jerszurki D, Saadon T, Zhen J, Agam N, Tas E, Rachmilevitch S, Lazarovitch N, 2021. Vertical microclimate heterogeneity and dew formation in semi-closed and naturally ventilated tomato greenhouses. Sci Hortic 288:110271.

Kang L, van Hooff T, 2024. Numerical evaluation and optimization of air distribution system in a small vertical farm with lateral air supply. Dev Built Environ 17:100304.

Liu TD, Song FB, 2012. Maize photosynthesis and microclimate within the canopies at grain-filling stage in response to narrow-wide row planting patterns. Photosynthetica 50:215-222.

Menter FR, 1994. Two-equation eddy-viscosity turbulence models for engineering applications. AIAA J 32:1598-1605.

Miyoshi Y, Hidaka K, Okayasu T, Yasutake D, Kitano M, 2017. Effects of local CO2 enrichment on strawberry cultivation during the winter season. Environ Control Biol 55:165-170.

Mochizuki Y, Murakami S, Kobayashi T, Worarad K, Yonezu Y, Umeda H, et al., 2022. Local CO2 application within strawberry plant canopy increased dry matter production and fruit yield in summer and autumn culture. Int J Fruit Sci 22:675-685.

Moon SM, Kwon SY, Lim JH, 2015. Improvement of energy efficiency of plants factory by arranging air circulation fan and air flow control based on CFD. J Internet Comput Serv 16:57-65.

Norton T, Sun DW, Grant J, Fallon R, Dodd V, 2007. Applications of computational fluid dynamics (CFD) in the modelling and design of ventilation systems in the agricultural industry: a review. Bioresour Technol 98:2386-2414.

Park JY, Yoo YJ, Kim YC, 2023. Optimization of the outlet shape of an air circulation system for reduction of indoor temperature difference. Sensors 23:2570.

Ryu HR, Choi EY, Choi KY, 2018. Growth characteristics, yield and fruit soluble carbohydrate content of hydroponically grown strawberry with carbon dioxide fertilization. Hortic Sci Technol 36:513-520.

Shamshiri RR, Kalantari F, Ting KC, Thorp KR, Hameed IA, Weltzien C, et al., 2018. Advances in greenhouse automation and controlled environment agriculture: a transition to plant factories and urban agriculture. Int J Agric Biol Eng 11:1-22.

Shin SH, Deb NC, Arulmozhi E, Tamrakar N, Ogundele OM, Kook J, et al., 2024. Prediction of carbon dioxide concentrations in strawberry greenhouse by using time series models. Agriculture 14:1895.

Sim HS, Kim DS, Ahn MG, Ahn SR, Kim SK, 2020. Prediction of strawberry growth and fruit yield based on environmental and growth data in a greenhouse for soil cultivation with applied autonomous facilities. Hortic Sci Technol 38:840-849.

Sohn J, Liulys M, Avgoustaki DD, Xydis G, 2023. CFD analysis of airflow uniformity in a shipping-container vertical farm. Comput Electron Agric 215:108363.

Sun P, Mantri N, Lou H, Hu Y, Sun D, Zhu Y, et al., 2012. Effects of elevated CO2 and temperature on yield and fruit quality of strawberry (Fragaria × ananassa Duch.) at two levels of nitrogen application. PLoS One 7.

Tagawa A, Ehara M, Ito Y, Araki T, Ozaki Y, Shishido Y, 2022. Effects of CO2 enrichment on yield, photosynthetic rate, translocation and distribution of photoassimilates in strawberry 'Sagahonoka'. Agronomy 12:473.

Teitel M, Atias M, Barak M, 2010. Gradients of temperature, humidity and CO2 along a fan-ventilated greenhouse. Biosyst Eng 106:166-174.

Wang X, Onychko V, Zubko V, Wu Z, Zhao M, 2023. Sustainable production systems of urban agriculture in the future: a case study on the investigation and development countermeasures of the plant factory and vertical farm in China. Front Sustain Food Syst 7:973341.

Yuce BE, Nielsen PV, Wargocki P, 2022. The use of Taguchi, ANOVA, and GRA methods to optimize CFD analyses of ventilation performance in buildings. Build Environ 225:109587.

Zhang Y, Kacira M, An L, 2016. A CFD study on improving air flow uniformity in indoor plant factory system. Biosyst Eng 147:193-205.

Zhang Y, Kacira M, 2022. Analysis of climate uniformity in indoor plant factory system with computational fluid dynamics (CFD). Biosyst Eng 220:73-86.
Zhang Y, Yasutake D, Hidaka K, Okayasu T, Kitano M, Hirota T, 2022. Crop-localised CO2 enrichment improves the microclimate, photosynthetic distribution and energy utilisation efficiency in a greenhouse. J Clean Prod 371:133465.

Contributions: Min Gyu Jung, investigation, methodology, software, validation, writing - original draft. **Md. Didarul Islam,** investigation, methodology, software, validation, writing - original draft. **Ji Min Jeong,** investigation, software, validation. **Byeong Jun Jeon,** methodology, resources, project administration. **Yong Kab Lee,** resources, software. **Min-Gyu Jeon,** methodology, writing - review & editing. **Hyoung-Ho Kim,** conceptualization, funding acquisition, supervision, writing - review & editing.
All authors contributed to the discussion, reviewed the manuscript, and approved the final version.

Conflict of interest: the authors declare that they have no known competing financial interests or personal relationships that could have appeared to influence the work reported in this paper.

Data availability statement: The datasets used and/or analyzed during the current study are available from the corresponding author on reasonable request.

Acknowledgments: This work was supported by the Technology Development Program (RS-2024-00468066) funded by the Ministry of SMEs and Startups (MSS, Republic of Korea). This work was also supported by the Glocal University 30 Project Fund of Gyeongsang National University in 2025.

Declaration of AI-assisted technologies in the writing process: During the preparation of this work, the authors used ChatGPT and QuillBot to improve language, clarity, and readability. After using these tools, the authors reviewed and edited the manuscript as needed and took full responsibility for the content of the published article.